Journal of
Marine Science and Engineering

MDPI

Article

Model Tests on the Frequency Responses of Offshore Monopiles

Rui He [1,2,*] and Tao Zhu [1,2]

[1] Key Laboratory of Coastal Disaster and Defense, Hohai University, Ministry of Education, Nanjing 210024, China; zhutaohhu@hhu.edu.cn
[2] College of Harbor, Coastal and Offshore Engineering, Hohai University, Nanjing 210024, China
* Correspondence: herui@hhu.edu.cn

Received: 30 September 2019; Accepted: 31 October 2019; Published: 26 November 2019



Abstract: Monopiles are widely used to support offshore wind turbines as a result of the extensive development of offshore wind energy in coastal areas of China. An offshore wind turbine is a typical high-rise structure sensitive to dynamic loads in ocean environment such as winds, water waves, currents and seismic waves. Most of the existing researches focus on elastic vibration analysis, bearing capacity or cyclic degradation problems. There're very few studies on vibration of monopiles, especially considering the influence of static loads with different amplitudes, directions, and loading-unloading-reloading processes. In this paper, laboratory-scale 1 g model tests for a monopile in dry sands were carried out to investigate the frequency responses of the monopile under different loading conditions. The bearing capacities of the model monopile were obtained as references, and dynamic loads and static loads with different amplitudes were then applied to the monopile. It was found that (1) the first resonant frequency of the monopile decreases with the increase of dynamic load amplitudes; (2) the first resonant frequency of the monopile steadily increases under the lateral static load and loading-unloading-reloading processes; (3) the frequency responses of the monopile with static loads in different directions are also quite different; (4) damping of the monopile is influenced by the load amplitudes, load frequencies, load directions and soil conditions. Besides, all the tests were conducted in both loose sand and dense sand, and the results are almost consistent in general but more obvious in the dense sand case.

Keywords: monopile; horizontal vibration; combined static and dynamic loads; different loading directions; frequency response functions

1. Introduction

Monopiles have been widely used in offshore wind engineering for their low costs, short construction periods and small environmental constraints. So, they are recommended by DNV (DET NORSKE VERITAS) code to be the well suited foundation type in the offshore wind power industry for water depths below 25 m [1]. Richards and Byrne [2] pointed out that 87% of the built foundations of offshore wind turbines are monopile foundations with large diameters. In recent years, monopiles are also widely used in Jiangsu, Zhejiang and other coastal areas of China where the surface layer of the seabed is mostly soft soil, while the bottom layer of the seabed is mainly fine sand.

Offshore wind turbines are typical high-rise and flexible structures with low natural frequencies, which can be very close to the frequencies of offshore dynamic loads such as winds, waves, currents and seismic waves (Figure 1a). As many studies have mentioned [3–7], the natural frequencies of offshore wind turbines should be controlled in a very narrow interval (1p–3p) to avoid the harm of resonances. Accordingly, vibration characteristics or dynamic impedances of pile foundations are of

great concern to designers. Numerous methods are available in the literature to obtain these vibration characteristics, including:

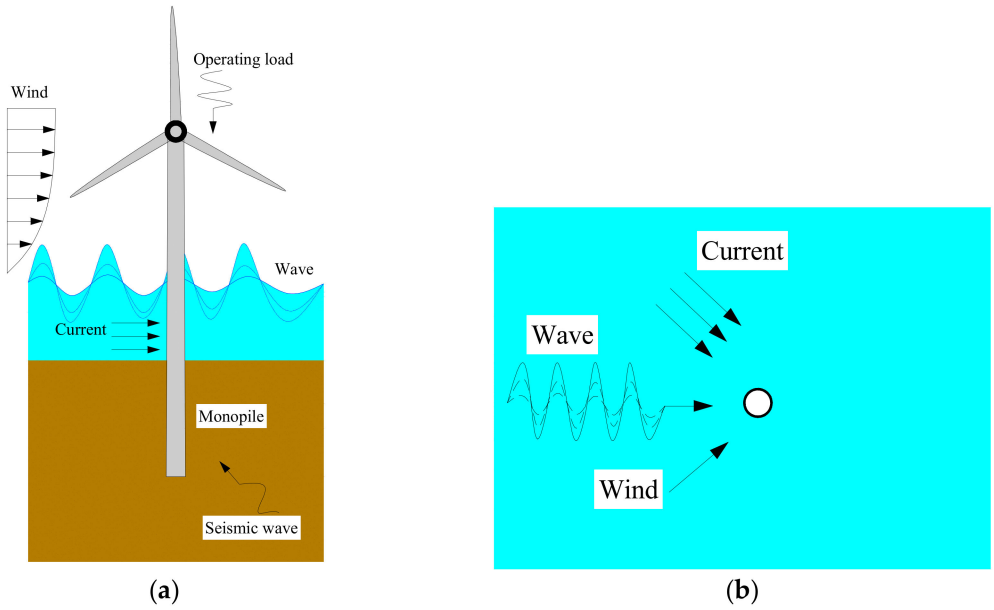


Figure 1. Loads on offshore wind turbines: (**a**) Front view; (**b**) Possible load direction from vertical view in water.

Analytic methods: Winkler type model—The soils around the pile are simplified into a series of independent 1D (one-dimensional) springs [8]; Plain strain model—The soils around the pile are treated as infinitely thin and independent 2D (two-dimensional) layers [9]; Virtual pile-soil model—The soil-pile system is decomposed into a fictitious pile and an extended 3D (three-dimensional) half-space [10]; Integral equation method, which is the most accurate analytical method to study 3D shell type foundations in offshore engineering—The theories of Cauchy singular and Fredholm integral equations are applied to solve the Green's function of pile and soil [11,12]; He et al. [13,14] obtained a rigorous analytical solution for coupled horizontal and rocking vibration of a monopile embedded in a porous seabed, and found that the effect of vertical shear stress on the monopile caused by horizontal loads and moments cannot be ignored.

Numerical methods: Zdravkovic et al. [15] presented a numerical study for laterally loaded monopiles; Sen et al. [16] presented a boundary element formulation for dynamic analysis of axially and laterally loaded single piles and pile groups; Latini and Zania [17] investigated the dynamic responses and the dynamic impedance of suction caissons by analyzing 3D finite element models in the frequency domain; Tao et al. [18] studied the influences of frequency, slenderness ratio, thickness–diameter ratio, soil–pile elastic modulus ratio and the existence of a scour hole on the dynamic impedances of monopile foundations; He et al. [19] analyzed the dynamic impedances and dynamic responses of large diameter rock-socketed monopiles under harmonic load based on a combined finite element–infinite element model; Ma et al. [20] presented a three-dimensional finite element model for analyzing the long-term performance of offshore wind turbines on monopiles in sand; Beuckelaers [21] brought insights into the behavior of monopile foundations and provided various modelling options to capture unloading, ratcheting and gapping effects for laterally loaded piles based on the Pile Soil Analysis (PISA) project.

Model experiments: Goit et al. [22] conducted dynamic experiments model soil–pile tests on a shaking table; Bhattacharya et al. [23] studied dynamic soil–pile interaction using a 1 g scale model test; Manna and Baidya [24] calculated the dynamic stiffness and damping of a slender pile and observed that the stiffness and damping decrease as the amplitude of load increases; Mohamed and Hesham [25] investigated the lateral vibration performance of two full-scale large-capacity helical piles and one driven pile installed in overconsolidated and structured clay, and observed a similar phenomenon

to Manna and Baidya [24]; Lombardi et al. [5] investigated changes in pile natural frequency and damping after 32,000–172,000 cycles of horizontal loading; He et al. [26] studied the decreases of the pile's natural frequencies with the existence of a scour hole; Futai et al. [4] measured the natural frequency of piles in centrifuge tests by FFT (Fast Fourier Transform), and investigated the influences of the density of sand and the ratio of free length to embedded depth; Leblanc et al. [27] carried out a series of laboratory tests where a stiff pile in dry sand was subjected to 8000–60,000 cycles of combined moment and horizontal loading, and presented the accumulated rotation and changes in stiffness after long-term cyclic loading; Richards et al. [2] presented results from laboratory tests in dry sand, which explored pile rotation with multidirectional cyclic loadings.

Full scale tests: Shirzadeh et al. [28] identified the damping values of an offshore wind turbine on a monopile foundation using both field measurements and simulations; Damgaard et al. [29] presented field vibration tests and numerical studies of the cross-wind dynamic properties of offshore wind turbines. Full scale tests are very significant but too expensive, and there are very few full scale tests that can be referred to.

The analytic methods [8–16] and numerical methods [17–19] mostly depend on the assumption that the soil is linear elastic so only the dynamic responses under small stress/strain conditions can be obtained, and the nonlinearity of soil is ignored. When considering the nonlinearity of soil, bearing capacity analysis [30–35] and accumulated deformation [36–39] under static/cyclic loads are mostly studied. However, the influence of the static loads on the dynamic behavior of the soil-pile system is very scarce. Actually, the offshore wind turbines are exposed to lateral loads caused by winds, water waves, currents and seismic waves with different load directions, as shown in Figure 1. These types of loads can be decomposed to combinations of static loads and dynamic loads, while the directions of the static loads and dynamic loads can also be different, and the effect of static load amplitudes and directions on the dynamic responses of monopiles is very important but rarely understood. Besides, extreme conditions, such as typhoons on the southeast coast of China, have a very significant impact on offshore structures as they can force monopiles to reach ultimate bearing conditions, but whether the dynamic characteristics of monopiles under such conditions change during this loading-unloading-reloading process is still unclear. As the stress-strain state of the soil around the monopile is very complicated under coupled loads, a model test is conducted to study these topics preliminarily, which aims to investigate how the frequency responses of the monopile change under different lateral static load cases, including loading-unloading-reloading processes. Compared with the existing researches, the novelty of this paper is that it studies the evolution of vibration characteristics of monopiles under complex loading conditions, which is rarely investigated at present.

2. Similitude Relationships

Appropriate scaling laws constitute the first step to deduce the results of a prototype from an experimental study. Based on a perfect scaling law, the prediction of the prototype may be carried out from results obtained in model tests. However, a coupled wind-wave-structure-soil system is involved in the study of offshore wind turbines, which means that almost no physical model test technology can concurrently satisfy all the physical interactions. Specific analysis is needed for concerned research targets. In this model test, the following physical parameters are considered, as shown in Table 1:

(1) Geometric parameters: He et al. [13] pointed out that the dynamic impedances of a monopile are related to the embedded aspect ratio L/D, the elastic modulus ratio between pile and soil (E_p/E_s) and the thickness–diameter ratio (h/D). The length–diameter ratio (L/D) of modern monopiles used in offshore wind turbines is very small, from 3 to 8. The thickness–diameter ratio (h/D) is about 0.01. As a result, the L/D of the model pile in the test is chosen as 5, and h/D is 0.01.

(2) E_p/E_s: For cohesionless soil, when the shear strain amplitude is less than 10^{-4}, the shear modulus G_0 is mainly related to the void ratio e and the average effective principal stress σ_m' [40]. For round sand ($e < 0.8$), G_0 can be estimated as

$$G_0 = 6934 \times \frac{(2.17 - e)^2}{1 + e} (\sigma_m')^2 \text{ kPa} \quad (1)$$

where e is the void ratio related to the relative density D_r. For fixed relative density, σ_m' is proportional to the depth h_s. The average elastic modulus of soil E_s is simplified to the elastic modulus of sand at the depth of around 0.5–1.0 D, for simplicity. The pile is made of steel E_p = 200 GPa, so $(E_p/E_s)_{\text{model}} \approx$ 10,000–20,000, while E_s in the prototype is about 10–250 MPa, with $(E_p/E_s)_{\text{prototype}} \approx$ 840–21,000, which means monopiles in both the model and prototype act like rigid piles. However, tests in loose sand (D_r = 10%, $E_p/E_s \approx$ 21,000) and dense sand (D_r = 88%, $E_p/E_s \approx$ 13,000) are conducted to investigate the influence of the elastic modulus ratio.

(3) Dimensionless frequency (a_0): According to soil dynamics, the responses are frequency-dependent, and the nondimensional frequency $a_0 = r\omega/\sqrt{\mu_s/\rho_s}$ is especially useful when analyzing the obtained results, where r is the radius of the pile, ω is the circular frequency of the load, μ_s is the shear modulus of the soil, and ρ_s is the density of the soil. a_0 has been chosen including 0–0.5 in accordance with most pile dynamic analysis works.

Table 1. Dimensionless characters in the test.

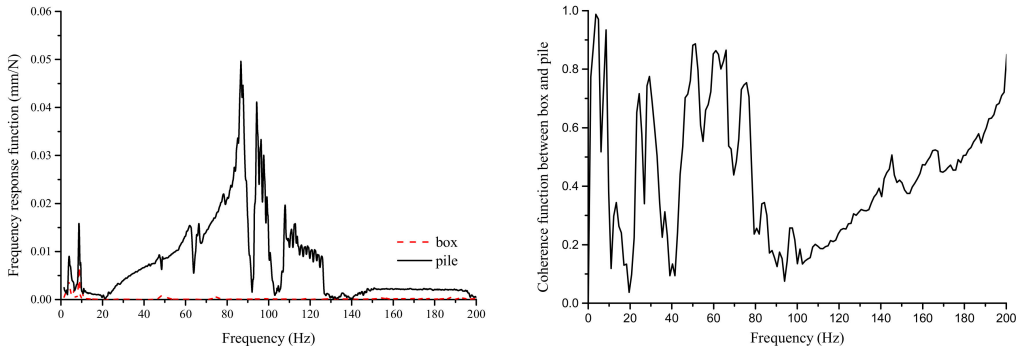
Physical Parameters	Dimensionless Characters	Value (D_r = 10%)	Value (D_r = 88%)
Embedded depth L	L/D	5	5
Wall thickness of the pile h	h/D	0.01	0.01
Elastic modulus E	E_p/E_s	21,000	13,000
Static load H	H/H_u	0–1.08	0–1.86
Harmonic load Amplitude H_{amp}	H_{amp}/H_u	1.35–27.03%	0.65–3.25%
Frequency f	$r\omega/\sqrt{\mu_s/\rho_s}$	0–0.72	0–0.56

3. Experimental Formulation

3.1. Test Platform

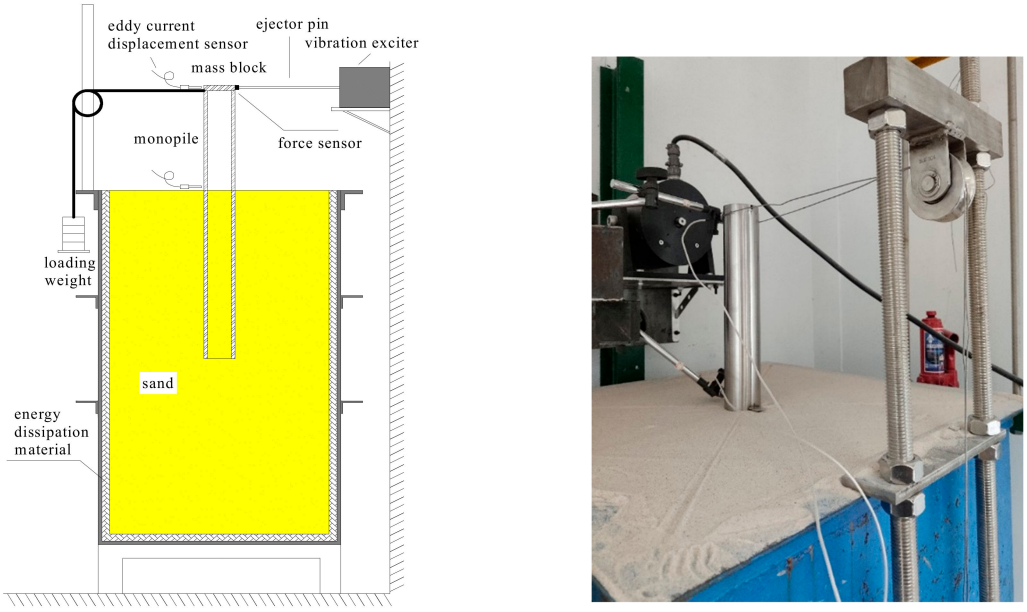
The experimental investigation was carried out in the Offshore Geotechnical Engineering Laboratory in Hohai University. Tests were conducted in an iron tank with the size of 600 × 600 × 1500 mm, which was filled with dry Nanjing quartz sand. The box was elevated above the ground to install a valve to release the sand in the box conveniently when the test was finished. A coherence analysis between the tank and the pile was carried out at first to ensure that the vibration of pile foundations is not affected by tank vibration (Figure 2).

The monopile foundation was scaled at around 1:50–1:100 to an open-ended steel model pile with diameter D = 60 mm, length L_0 = 600 mm, and wall thickness h = 0.6 mm; both the free length and the embedded depth were L = 300 mm (L/D = 5). To simulate the mass of the nacelle, an iron block was welded on the top of the pile. In addition, the pile was placed in the center of the box by the hammer-driven method. The lateral dynamic load was applied by a vibration exciter, which can exert harmonic loads, sweeping loads and random loads (Figure 3).



(a) (b)

Figure 2. The influence of tank vibration: (**a**) Frequency response functions of the soil tank and the pile; (**b**) Coherence function between the soil tank and the pile.



(a) (b)

Figure 3. Experimental setup and sensor placement: (**a**) Sketch of the model; (**b**) Photo of the model.

3.2. Test Series

The following series of tests were included in the test process, as shown in Table 2:

(1) LBC: the lateral bearing capacity test in loose sand (D_r = 10%, L.LBC) and dense sand (D_r = 88%, D.LBC).

(2) HL: vibration characteristic test of monopile foundation under harmonic loads with different amplitudes. Harmonic loads with different frequencies and fixed amplitudes are applied to the pile top, and the displacements and the loads are measured. Then, change the amplitude of the loads from 1 N to 5 N in the dense sand case, and from 0.5 N to 10 N in the loose sand case.

(3) SL: the influence of the lateral static load on the vibration characteristics by hammer excitation with FRF method.

(4) L-U: three repeated loading-unloading processes to comprehend how extreme static loads influence the vibration characteristics of the pile.

(5) S-D: the influence of the static load on the vibration characteristics in different directions.

Table 2. Test series.

Test Name	D_r	f (Hz)	Dimensionless Frequency a_0	Amplitude H_{amp} (N)	H_{amp}/H_u	Static Load H (N)	H/H_u
L.LBC	10%	0	0	-	-	0–40	0–1.08
D.LBC	88%	0	0	-	-	0–165	0–1.06
L.HL	10%	40–200	0.14–0.72	1/2/3/4/5	0.65–3.25%	0	0
D.HL	88%	40–200	0.11–0.56	0.5/1/1.5/2/2.5	1.35–6.75%	0	0
	88%	40–50 100–200	0.11–0.14 0.28–0.56	4/6/8/10	10.81–27.03%	0	0
L.SL	10%	Random		Hammering	-	0–40	0–1.08
D.SL	88%					0–290	0–1.86
L.L-U	10%	Random		Hammering	-	0–20	0–0.54
D.L-U	88%					0–100	0–0.64
L.S-D1	10%	Random		Hammering	-	0	0
L.S-D2	10%					8	0.22
L.S-D3	10%					16	0.43
D.S-D1	88%					0	0
D.S-D2	88%					40	0.26
D.S-D3	88%					80	0.51

3.3. Preparation of the Sand

For the quartz sand used in the tests, the particle size is 0.2–0.6 mm, with the medium diameter 0.42 mm, minimum density 1.35 g/cm^3, and maximum density 1.57 g/cm^3. The gradation curve is shown in Figure 4. The friction angle of the sand is about 30°.

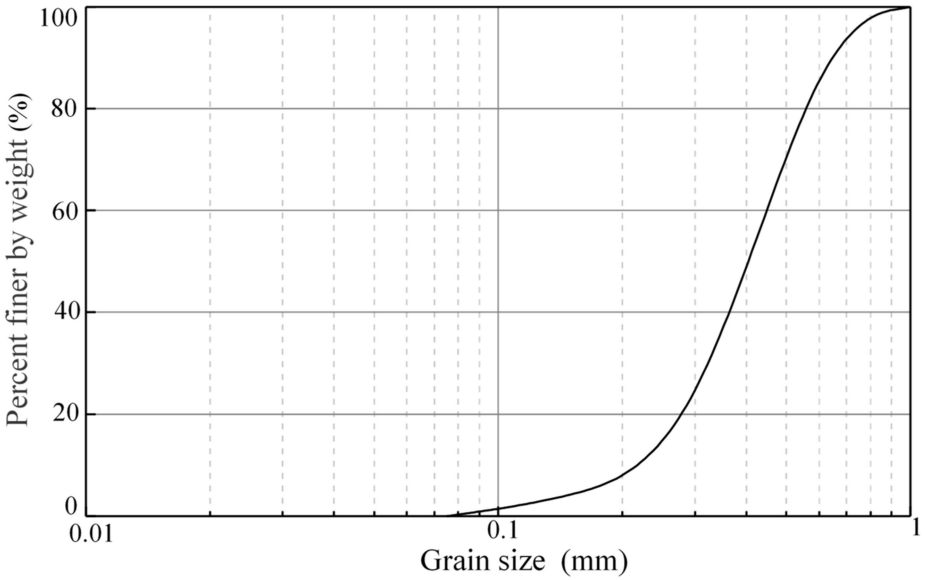


Figure 4. Gradation curve.

For sand, relative density D_r is of great importance in geotechnical tests [41]. The test will be more credible and repeatable if the relative density of the sand is well controlled. Various methods are used in the laboratory to reconstitute the sand, including pluviation, vibration and tamping. Pluviation through air is the most preferred method for its similarity to natural sand in the deposition mode [42]. According to the research now available, when other conditions remain unchanged, the relative density of sand is positively correlated with the falling distance [43].

In this paper, an experimental equipment of stationary pluviation was made referring to Chennarapu's method [43]. As shown in Figure 5, this device consists of three layers of sieves. The diameter of the sieve hole of the first layer (made of Acrylic plate) is 10 mm, and it has two layers

(sheet1, sheet2) close together. When the sieve holes in each layer are staggered, the sieve can be filled with sand. When the sieve holes are aligned, the sand will flow out. The second layer (sheet3) and the third layer (sheet4) are made of stainless steel and the diameters of the sieve holes are 6 mm and 3 mm, respectively. To adjust the falling distance, the sieve is hung on a fixed pulley.

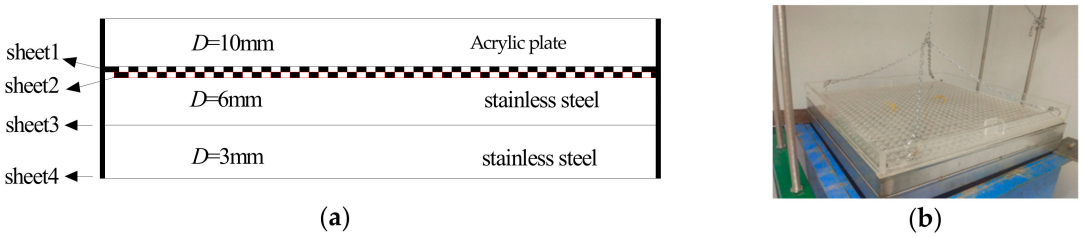


Figure 5. Pluviation equipment: (**a**) Sketch of the equipment; (**b**) Photo of the equipment.

The relationship between the falling distance h_f and the relative density D_r of the sand was observed before the experiment. As shown in Figure 6, nine sampling boxes are arrayed in the tank. After the boxes are overflowed by the soil, the relative density of the soil in the box is measured. To ensure that this device is reliable, 18 times' test results with the falling distance 30 cm were obtained, as shown in Figure 6.

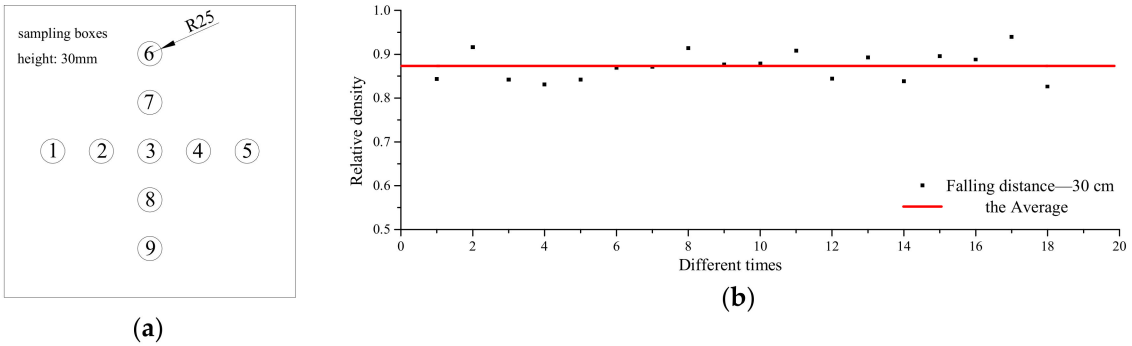


Figure 6. Relative density with the falling distance 30cm: (**a**) Sampling boxes; (**b**) Test reliability.

Finally, the relationship between h_f and D_r was mapped, and the falling distance can be found in Figure 7, where soil with relative density 0.75–0.9 is in need.

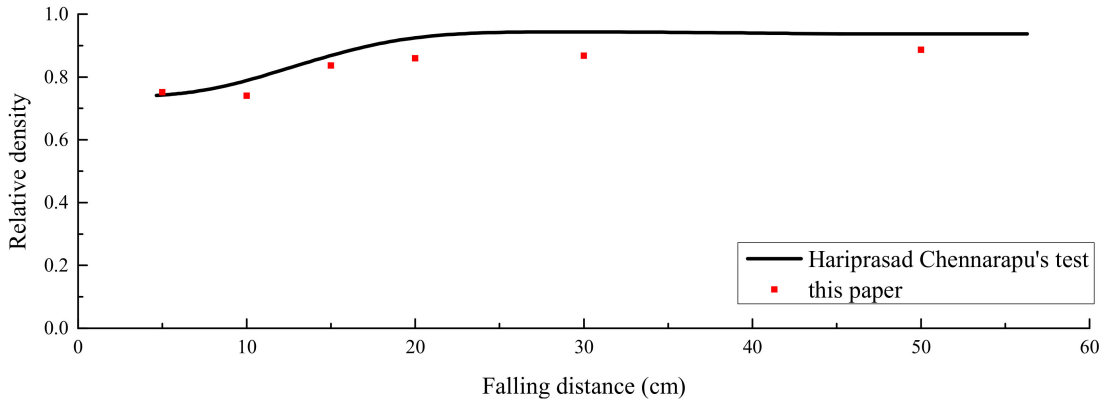


Figure 7. Relationship between the falling distance and the relative density.

On the other hand, loose sand was prepared by manual pouring from a very low height to achieve a density of $\rho_L = 1.39 g/cm^3$, and the corresponding relative density is 10%.

4. Test Results

4.1. Horizontal Bearing Capacity

In this paper, the horizontal bearing capacity of the monopile foundation (H_u) was obtained as a reference of the dynamic load amplitudes. According to Cuéllar et al. [44], the ultimate bearing capacity of a pile foundation under horizontal static load can take the corresponding load when the displacement of the pile top reaches 0.1 D. According to the Code for Pile Foundation in Port Engineering [45], the loading process is divided into 10 stages, and 0.1 Hu is loaded each time. When the displacement evolution rate at the loading point is less than 1×10^{-5} m/min in 30 minutes, start the next loading stage. Stop loading when total displacement reaches 0.1 D. From Figure 8, it can be found that the displacements are stable after each load. From Figure 9a, it can be found that the horizontal bearing capacity H_u is about 156 N and 37 N for dense sand and loose sand, respectively. The corresponding evolution of the rotation angle is also shown in Figure 9b.

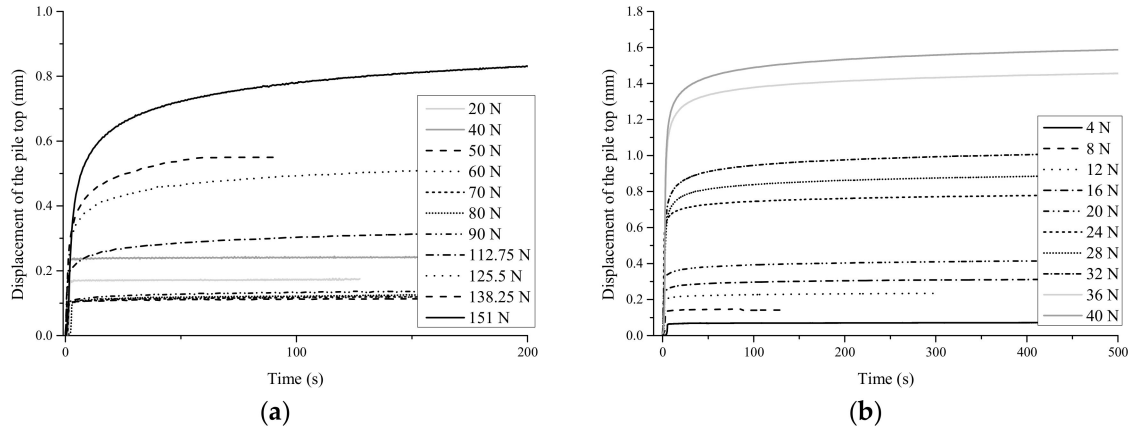


Figure 8. Y-T curves: (**a**) Dense sand case; (**b**) Loose sand case.

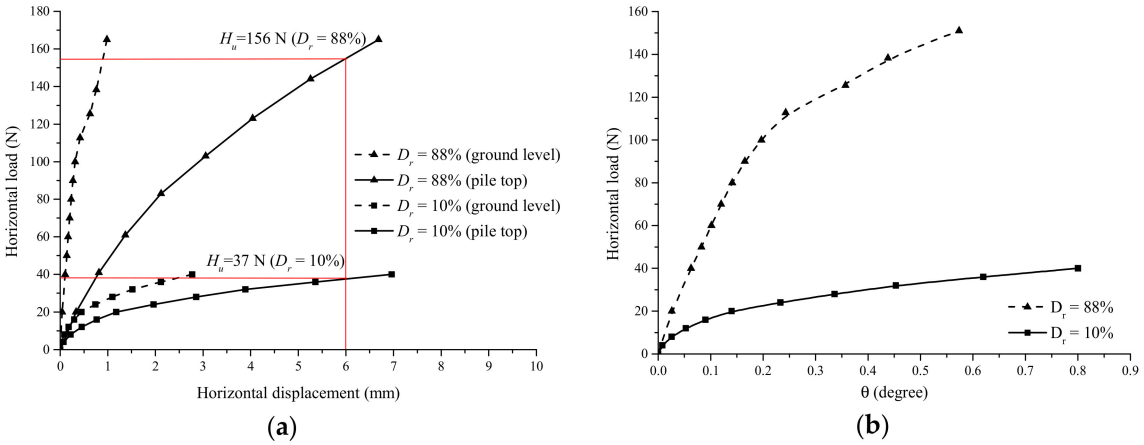


Figure 9. Horizontal bearing capacity: (**a**) Force - horizontal displacement curve; (**b**) Force- rotation angle curve.

4.2. Vibration Characteristics under Dynamic Loading with Different Amplitudes

Research on the influence of load amplitudes on the vibration characteristics of traditional slender piles has been well studied, but there are very few results for rigid monopiles. In this section, harmonic loads with different frequencies from 40 Hz to 200 Hz are applied on the top of the pile, and the test group is repeated with different amplitudes from 1 N to 5 N (dense sand, 0.65%H_u–3.25%H_u), from 0.5 N to 2.5 N (loose sand, 1.35%H_u–6.75%H_u). Harmonic loads with amplitudes of 4–10 N (10.81%H_u–27.03%H_u) are applied on the pile in loose sand to study the influences of soil nonlinearity.

Actually, it would be more realistic if the amplitude of the harmonic load in the test could reach 30% H_u or more because the cyclic load in the ocean can reach 30% of the ultimate bearing capacity. However, when the load amplitude was large enough and the frequency of the load was near the natural frequency, the sand around the pile vibrated violently and flowed toward the center so that the properties of the sand were different and the results cannot be put together for comparison. Time-domain sampling data under harmonic load with frequency 120 Hz and amplitude 5N are shown in Figure 10a. The displacement is obtained when it is stable (Figure 10b), and the loading time should be as short as possible to avoid the densification of the sand.

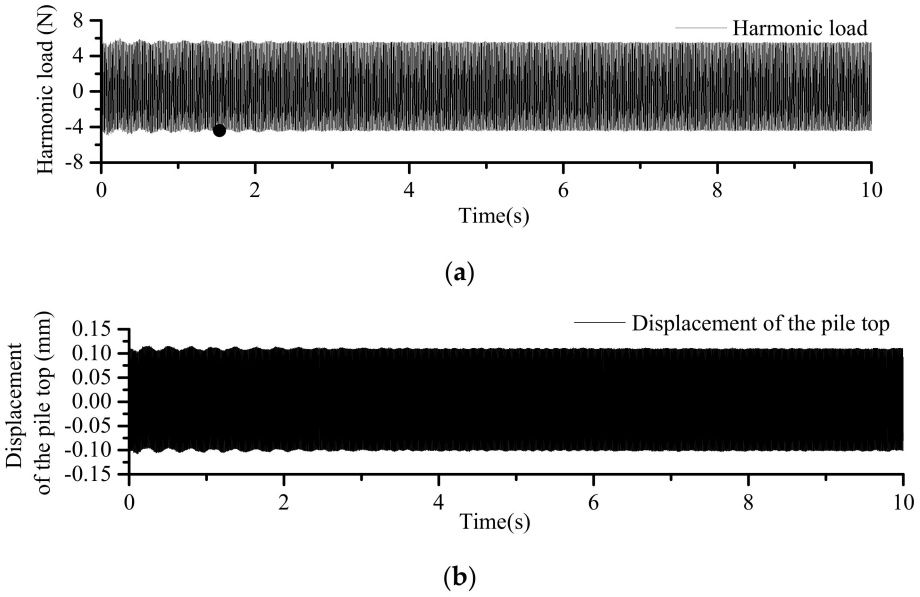


Figure 10. Time-domain sampling: (**a**) Harmonic load; (**b**) Displacement of the pile top.

Figures 11 and 12 show the frequency response curves of the monopile with different dynamic load amplitudes. The natural frequency decreases with the increase in the dynamic load amplitude H_{amp} in both dense sand and loose sand. In Figure 12b, H_{amp}/H_u is up to 27.03%, but the response is too large to be captured when the loading frequency is around the first natural frequency. According to the knowledge of structural dynamics, the natural frequency f_1 and stiffness K are positively correlated, and K is bound up with the shear modulus G of the soil. Hardin and Drnevich [46] obtained a negative correlation between the shear modulus and strain of sand by tests. Therefore, natural frequency decreases with the increase in the load amplitude, as Figure 13 shows. When H_{amp}/H_u is 0–4%, f_1 decreases with H_{amp}/H_u linearly; when H_{amp}/H_u is larger, the curve enters the nonlinear segment for the loose sand case. According to structural dynamics [47], the damping ratio of the pile can be obtained as $\xi = \frac{f_b - f_a}{2f_1}$ (Figure 14a), where f_1 is the frequency corresponding to the peak of the frequency response function curve (FRF_{max}), and f_a and f_b are the frequencies corresponding to $FRF_{\max}/\sqrt{2}$. The obtained damping ratio of the monopile in the model test is given in Figure 14b, and it can be found that the damping ratio increases with the increase in load amplitudes during both dense sand and loose sand cases.

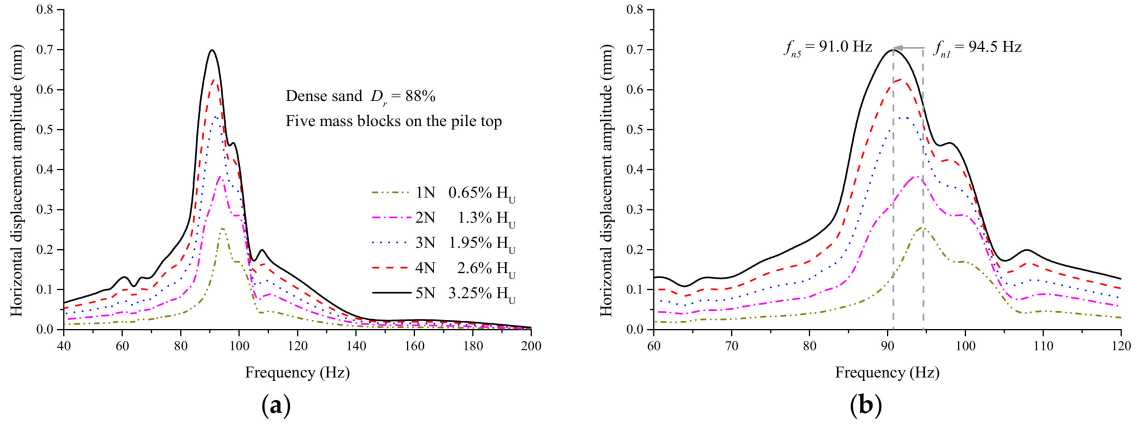


Figure 11. Horizontal displacement amplitudes with different load amplitudes and frequencies in dense sand: (**a**) 40–200 Hz; (**b**) 60–120 Hz.

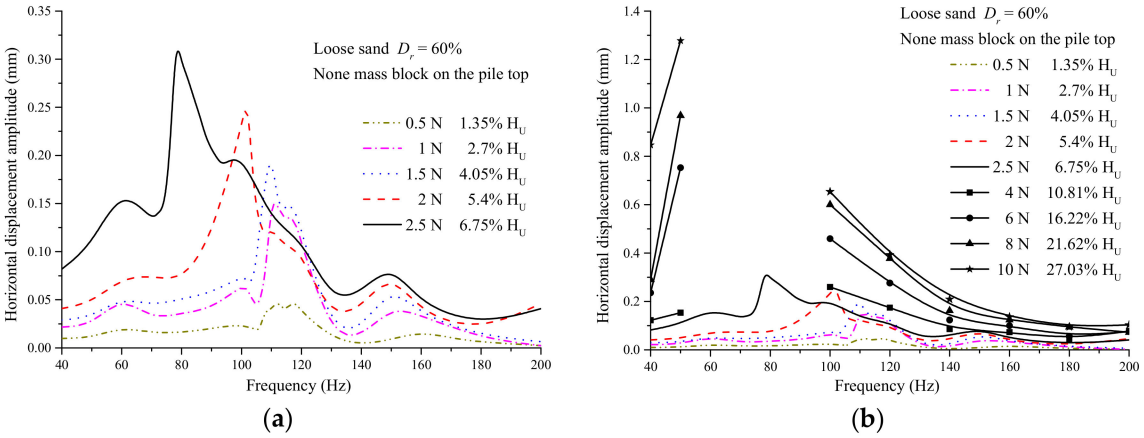


Figure 12. Horizontal displacement amplitudes with different load amplitudes and frequencies in loose sand: (**a**) 0.5–2.5 N; (**b**) 0.5–10 N.

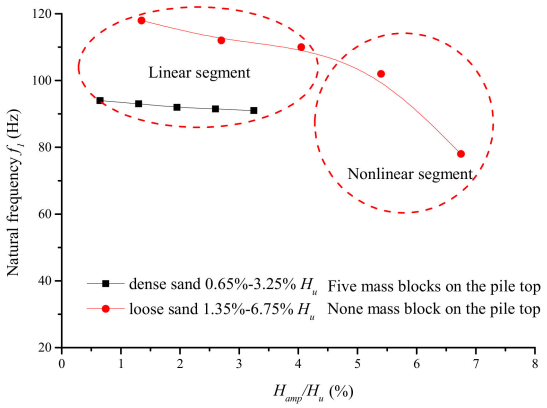


Figure 13. Influence of H_{amp}/H_u on natural frequency f_1.

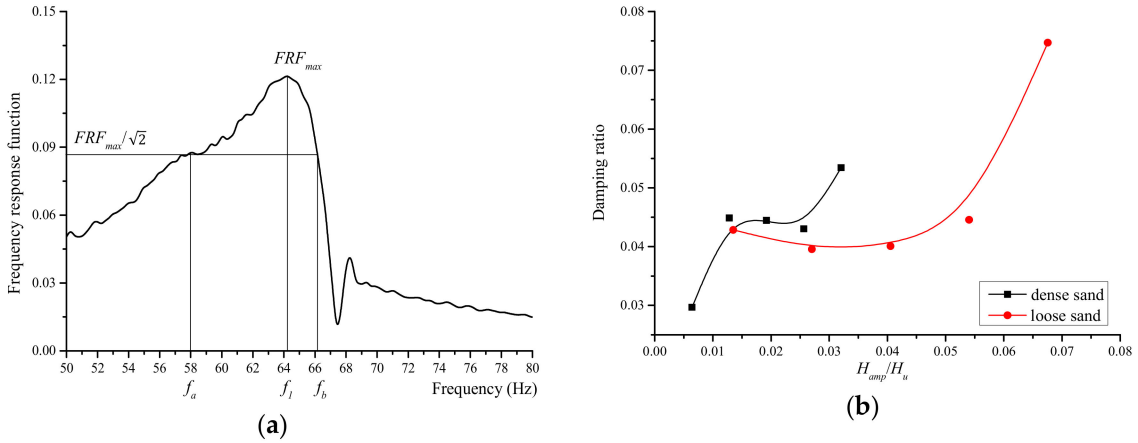


Figure 14. Calculation of damping ratio: (**a**) Method; (**b**) Model test results.

4.3. Vibration Characteristics under Different Static Loads

Few studies are concerned with the vibration characteristics under different lateral static loads; however, in the coastal areas of China where typhoons are frequent, it is important to study the vibration characteristics of monopile foundations under extreme loads.

In this section, hammer excitation was exerted on the pile top and frequency response analysis (FRA) was applied to obtain the vibration characteristics. In order to ensure the reliability of the hammering method, a comparison with random excitation was carried out, and the two results coincide well, as shown in Figure 15. Figure 16 shows the frequency response functions of the pile with different lateral static loads. Figure 17 shows the relationship between frequency and lateral static load, and the color of the pictures represents the ratio of *FRF* (frequency response function) to FRF_{max} (the maximum value of each frequency response curve), which helps us observe the peaks of the curves clearly, and the increasing of f_1 with the increase of the static load can be obtained.

Similar results occur in both the loose sand case and dense sand case, where f_1 increases under the loading process by and large. It can be obtained from Figure 17a that f_1 increases until static load is 220 N (much larger than the static bearing capacity 154 N) in the dense sand case. In Figure 17b, there are two distinct resonance frequencies, f_1 and f_2, in the loose sand case, which are caused by the horizontal vibration and rocking rotation of the monopile when the constraint supplied by the soil is insufficient. The first resonance frequency increases with the increase in static load, as in the dense sand case. However, the second resonance frequency almost keeps the same during the loading process.

The reason for the increase in the first natural frequency under static load is thought partly due to the increase in the shear modulus G of soils around the monopile. As Seed and Idriss [48] pointed out, the shear modulus G_0 of sand is positively correlated with confining pressure. As shown in Figure 18, the average stress around the monopile along the loading direction will be larger under static load than no static load case [49]. When the static load increases to a certain extent, the sand gradually reaches the limit state, and the resonance frequency decreases. On the other hand, it should be noted that the change of natural frequency may partly due to the constraint of the wire rope and the inertia of the added balance weights (the static force is exerted by the wire rope and balance weights). For monopiles in ocean environment, part of the forces are due to inertial effects (refer to Morison's equation for wave loading), which is similar to the case in this study, to some extent. However, further tests in a flume or in the field are needed to verify the results obtained here, and the contributions of the two parts should also be separated in future. This preliminary phenomenon states that the resonance frequency of the wind turbine may still be changing under horizontal static loads or even extreme loads. So, it is necessary to be concerned about the occurrence of resonance even during the ultimate bearing capacity design state.

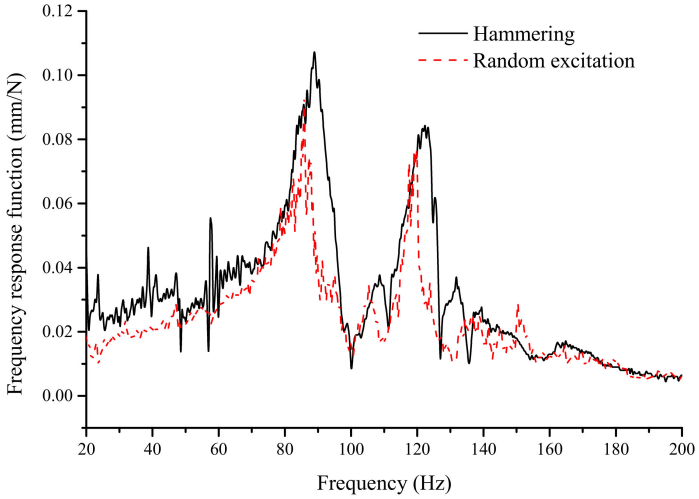
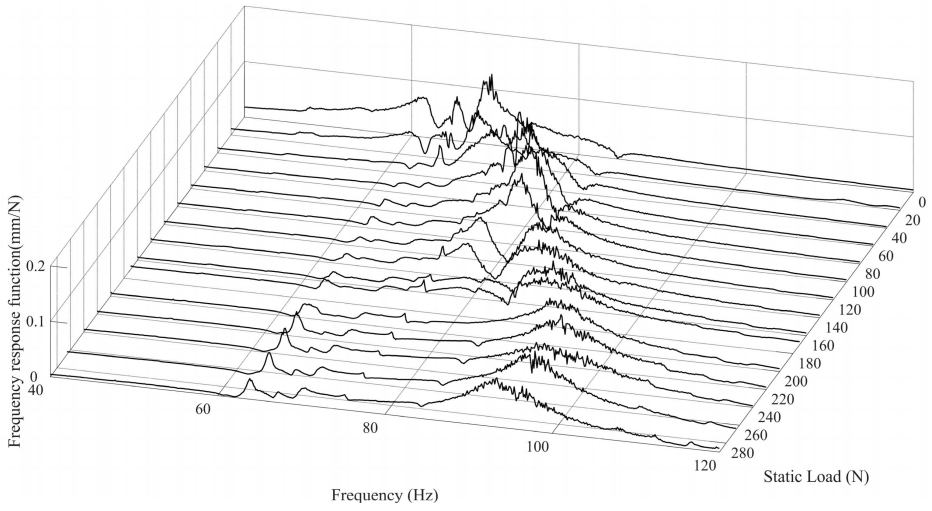
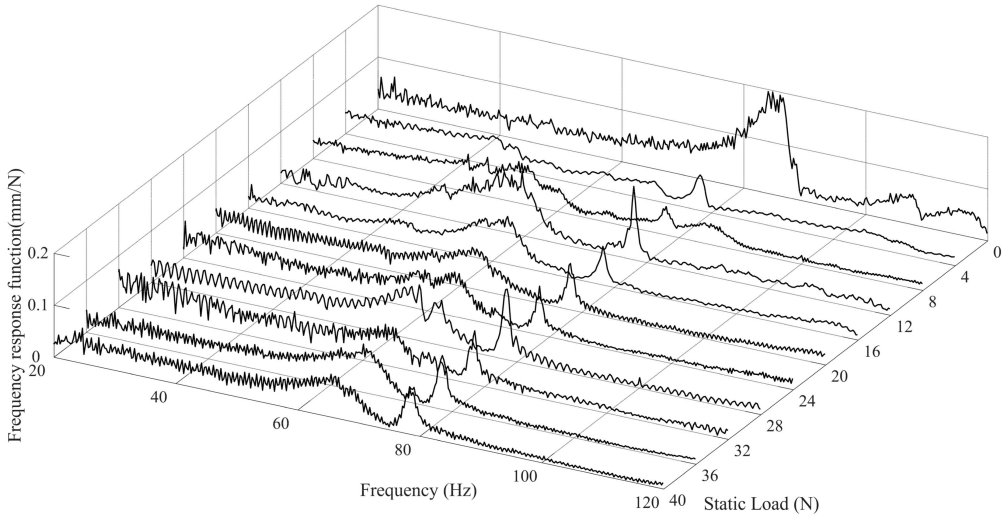


Figure 15. Frequency response functions of hammering and random excitation.



(**a**)



(**b**)

Figure 16. Frequency response functions of the pile with different lateral static loads: (**a**) Dense sand; (**b**) Loose sand.

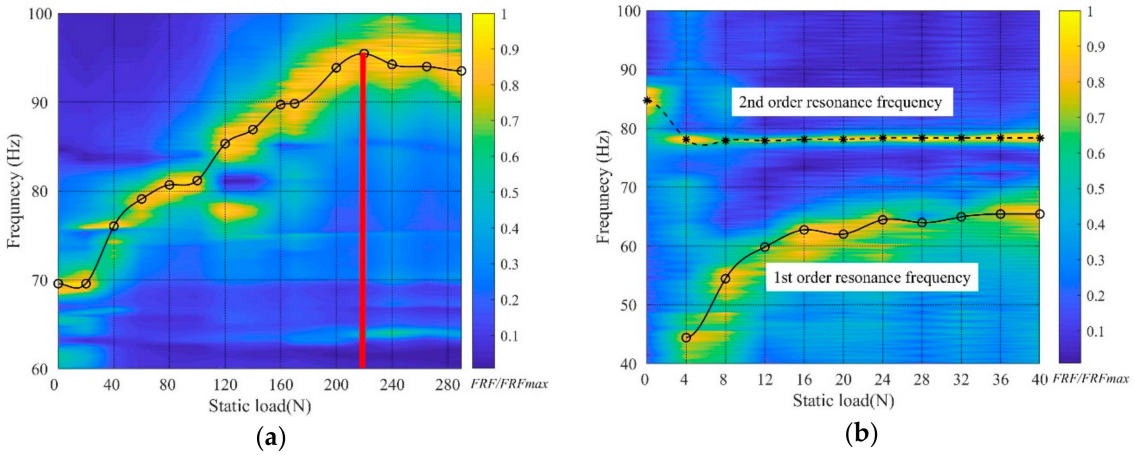


Figure 17. The relation between resonant frequencies and lateral static load: (**a**) Dense sand case; (**b**) Loose sand case.

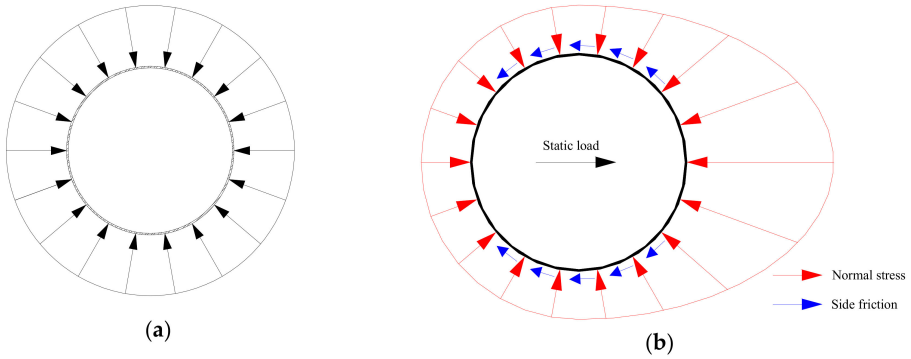


Figure 18. Stresses of soil around the pile: (**a**) No static load; (**b**) with static load.

Furthermore, the change in frequency responses during the loading-unloading-reloading process is shown in Figures 19 and 20. It can be observed from Figure 19 that the natural frequencies of the unloading process are larger than those of the loading process; the natural frequencies of the loading starting points and finishing points all increase after each loading and unloading process in dense sand case. However, this phenomenon is not obvious in loose sand case (Figure 20), but it proves the repeatability of the phenomena in Figure 17b.

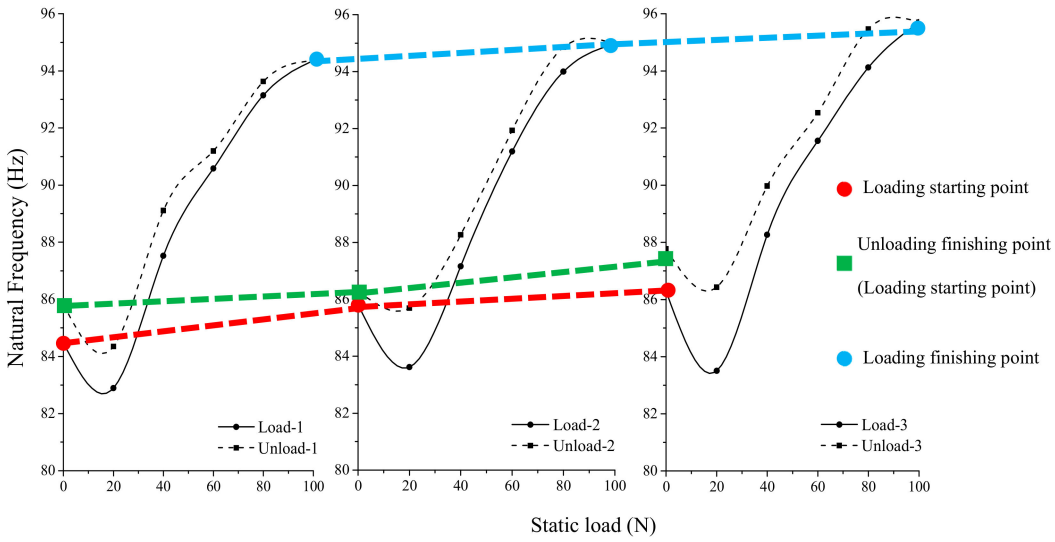


Figure 19. The influence of the loading and unloading process on natural frequency in dense sand.

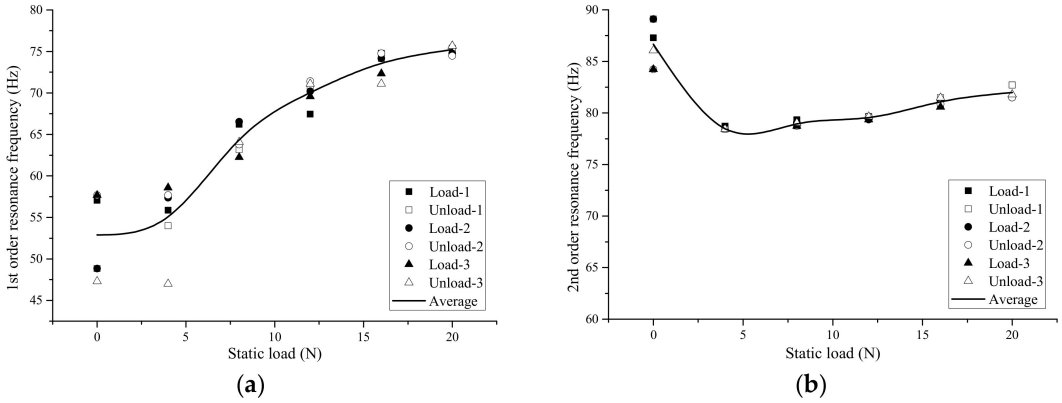


Figure 20. The influence of the loading and unloading process on natural frequency in loose sand: (**a**) First order resonance frequency f_1; (**b**) Second order resonance frequency f_2.

4.4. Vibration Characteristics in Different Directions under Different Static Loads

The directions of loads such as wind, waves and current are not always the same, and the foundation can vibrate in different directions. For simplicity, it is useful to study the vibration characteristics of the monopile in different directions under the main static loads. In this section, static load was applied to the top of the pile in DIR-1, and the hammer excitation was exerted in DIR-1, DIR-2, DIR-3, and DIR-4, respectively. The displacements were acquired in four directions by displacement sensors simultaneously, as shown in Figure 21. Based on the fundamental principle of modal analysis, the FRF curves of four directions were obtained under the condition that the pile is loaded in DIR-1 by static load (0 N, 40 N, and 80 N in dense sand case, and 0 N, 8 N, and 16 N in loose sand case, respectively).

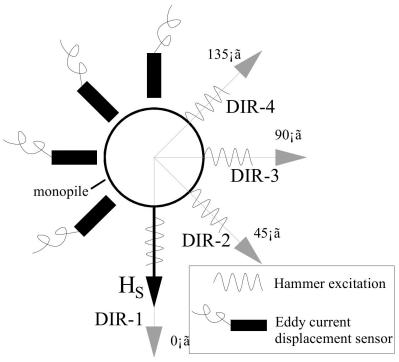


Figure 21. Layout of this experiment.

The results for dense sand case and loose sand case can be found in Figures 22 and 23, respectively. In this section, the results in dense sand are mainly analyzed, while the results in the loose sand case are similar, although not so obvious as in dense sand case.

As mentioned in the previous section, the first frequency f_1 of DIR-1 increases as expected with the increase of the static load in DIR-1. This proves once again that the stiffness provided by the soil-pile system increases with the increase in horizontal static load. However, it is different in DIR-3, which is perpendicular to DIR-1, where f_1 almost remains unchanged with the increase in the static load, but the amplitude of the FRF curve increases, which means a decrease in the damping ratio of the pile in DIR-3, as shown in Figure 24a. Damping ratio here is composed of two parts: the radiative damping, which increases with the increase in frequencies, and decreases with load amplitudes; and the material damping, which increases with the soil nonlinearity. The results for DIR-2 and DIR-4 lie between the results for DIR-1 and DIR-3. Theoretically, the results of DIR-2 and DIR-4 should be similar, and this is true from a general point of view.

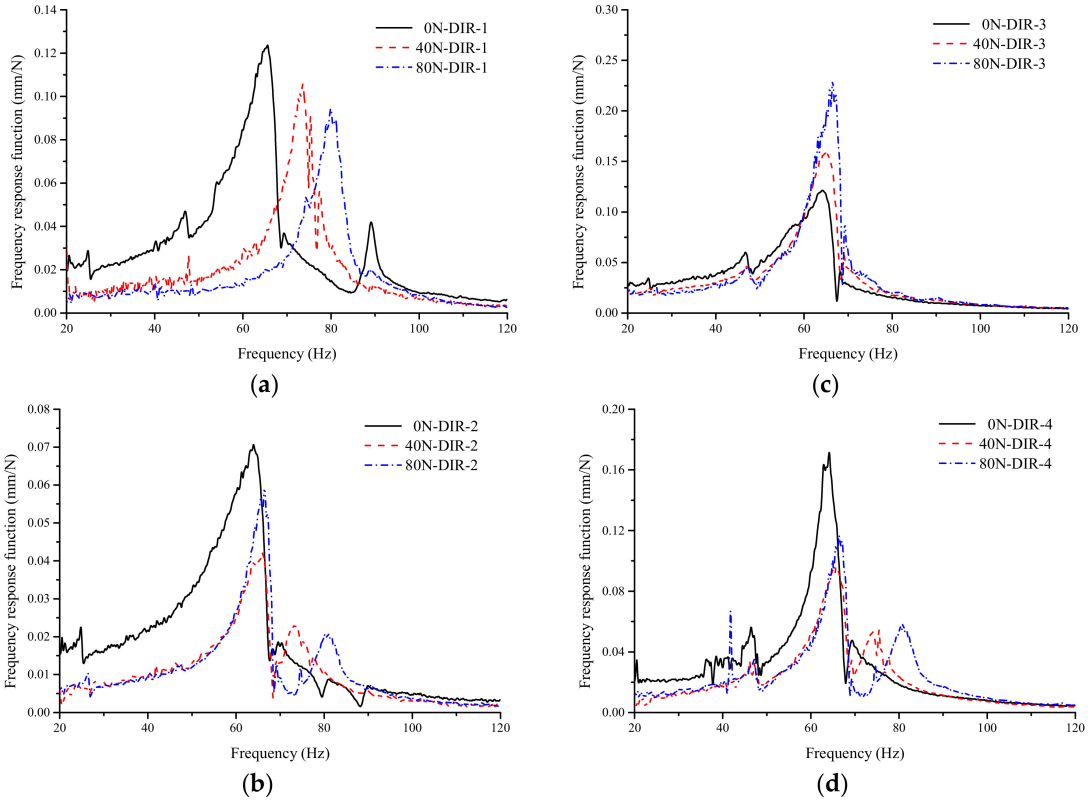


Figure 22. Frequency response functions of different directions under different lateral static loads: (**a**) Direction-1; (**b**) Direction-2; (**c**) Direction-3; (**d**) Direction-4.

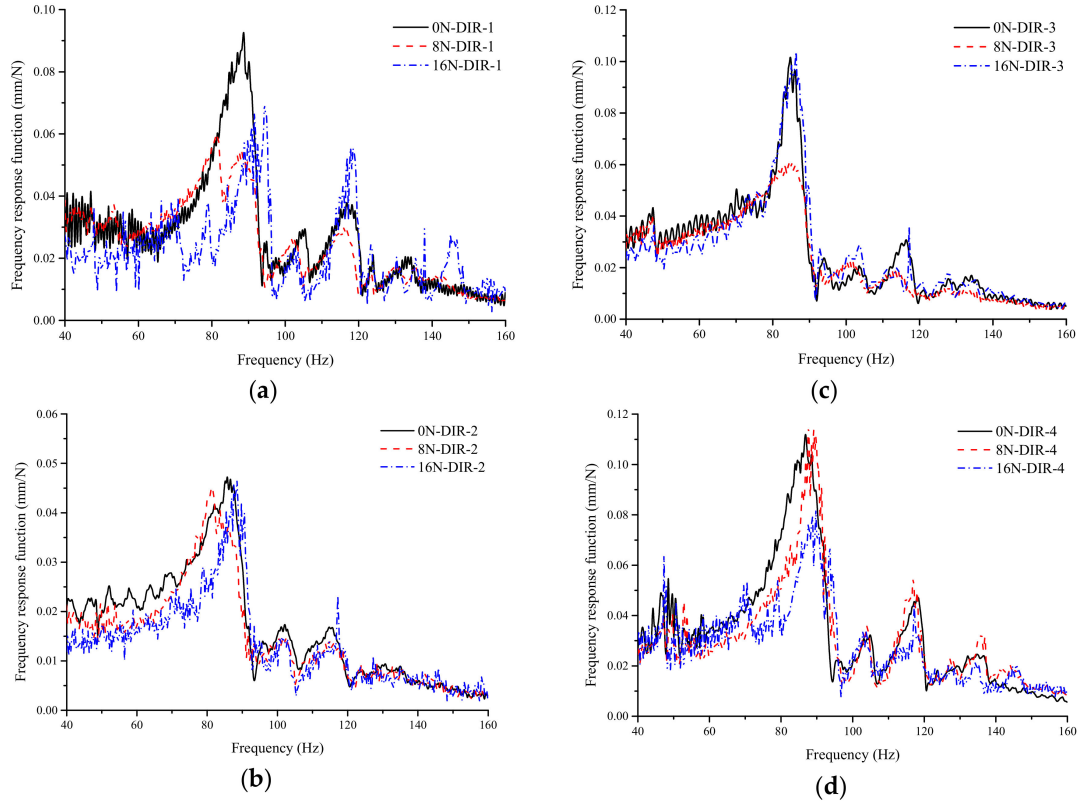


Figure 23. Frequency response functions of different directions under different lateral static loads in loose sand: (**a**) Direction-1; (**b**) Direction-2; (**c**) Direction-3; (**d**) Direction-4.

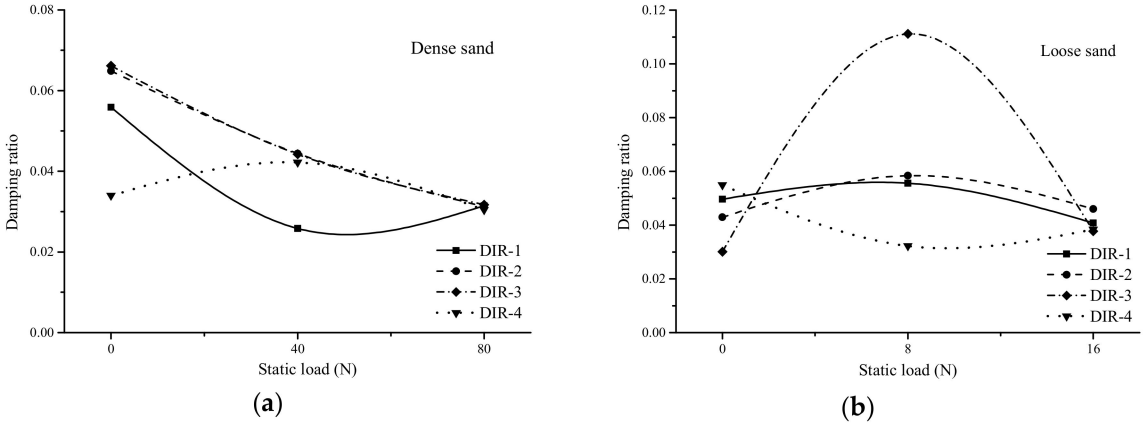


Figure 24. Total damping ratio of the model monopile: (**a**) Dense sand case; (**b**) Loose sand case.

Based on the results above, the differences of dynamic stiffness and damping in different directions should be focused on when the directions of the wind, waves or current are crossed.

5. Conclusions and Outlook

5.1. Conclusions

In this paper, the results of laboratory-scale 1 g model tests for monopiles in dry sands (D_r = 10% and 88%) are presented. The vibration characteristics of the model monopile under different lateral loading amplitudes, directions and loading-unloading cycles are analyzed by the FRF method. The main conclusions are:

(1) When there is no static load, the first natural frequency f_1 decreases with the increase of the amplitudes of the dynamic loads in both dense sand and loose sand cases;
(2) The first natural frequency f_1 increases with the increase in the lateral static load generally in both the dense and loose sand cases; Loading-unloading-reloading to the capacity process can increase the first resonance frequency of the monopile in dense sand, but this phenomenon is not observed in loose sand case;
(3) The frequency responses of the monopile in the direction perpendicular to the static loading are quite different from those in the static loading direction, as soils around the monopile are under different stress conditions, and this is more obvious in the dense sand case.

5.2. Outlook

In this study, several simplifications were used: the blades and nacelle on the top of the monopile are simplified as mass blocks; the stress level of soil is lower than the field case, and it is only taken as guaranteed that both the monopiles behave like rigid ones; the full drainage condition of saturated sand is modeled as dry sand. In order to further study the vibration characteristics of monopiles of offshore wind turbines, different seabed geological conditions, soil stress levels, drainage conditions, and actual wave, current and wind loads should be taken into account. Besides, theoretical or numerical models that can explain the observed results should be developed.

Author Contributions: Conceptualization, supervision, R.H.; model test, writing—original draft, T.Z.; data analysis, writing—review & editing, R.H. and T.Z.

Funding: The authors would like to acknowledge Grant No. 51879097 from the support of the National Natural Science Foundation of China, the Grant No. BK20190074 from the Natural Science Foundation of Jiangsu Province, and the Grant No. 2019B53114 and 2018B12714 from Fundamental Research Funds for the Central Universities.

Conflicts of Interest: The authors declare no conflict of interest. Rui He and Tao Zhu.

Nomenclature

L	embedded length of the monopile	H	horizontal static load
D	diameter	H_{amp}	harmonic load amplitude
E_p	elastic modulus of the monopile	H_u	ultimate bearing capacity of the pile
E_s	elastic modulus of soil	ρ_s	soil density
h	thickness of the monopile	L_0	length of the monopile
G_0	initial shear modulus of soil	f	load frequency
e	void ratio	h_f	falling distance
$\sigma_m{}'$	average effective principal stress	ρ_L	density of loose sand
h_s	soil depth	K	stiffness of structure
D_r	relative density	ξ	damping ratio
a_0	dimensionless frequency	$FRFmax$	peak of the FRF curve
r	radius of the monopile	f_1	first order resonance frequency
ω	circular frequency	f_a, f_b	the frequencies corresponding to $FRFmax/\sqrt{2}$
μ_s	shear modulus of soil	f_2	second order resonance frequency

References

1. DNV. *Offshore Standard DNV-OS-J101: Design of Offshore Wind Turbine Structures*; DNV: Oslo, Norway, 2010.
2. Richards, I.A.; Byrne, B.W.; Houlsby, G.T. Monopile rotation under complex cyclic lateral loading in sand. *Géotechnique* **2019**. [CrossRef]
3. Krolis, V.D.; Zwaag, G.L.V.D.; Vries, W.D. Determining the embedded pile length for large-diameter monopiles. *Mar. Technol. Soc. J.* **2010**, *44*, 24–31. [CrossRef]
4. Futai, M.M.; Dong, J.; Haigh, S.K.; Madabhushi, S.P.G. Dynamic response of monopiles in sand using centrifuge modelling. *Soil Dyn. Earthq. Eng.* **2018**, *115*, 90–103. [CrossRef]
5. Lombardi, D.; Bhattacharya, S.; Muir Wood, D. Dynamic soil-structure interaction of monopile supported wind turbines in cohesive soil. *Soil Dyn. Earthq. Eng.* **2013**, *49*, 165–180. [CrossRef]
6. Damgaard, M.; Bayat, M.; Andersen, L.V.; Ibsen, L.B. Assessment of the dynamic behaviour of saturated soil subjected to cyclic loading from offshore monopile wind turbine foundations. *Comput. Geotech.* **2014**, *61*, 116–126. [CrossRef]
7. Leblanc, C. Design of Offshore Wind Turbine Support Structures: Selected topics in the field of geotechnical engineering. Ph.D. Thesis, Aalborg University, Aalborg, Danmark, 2009.
8. Dobry, R.; Gazetas, G. Dynamic response of arbitrarily shaped foundations. *J. Geotech. Eng.* **1986**, *112*, 109–135. [CrossRef]
9. Novak, M.; Nogami, T. Soil-pile interaction in horizontal vibration. *Earthq. Eng. Struct. D* **1977**, *5*, 263–281. [CrossRef]
10. Muki, R.; Sternberg, E. On the diffusion of an axial load from an infinite cylindrical bar embedded in an elastic medium. *Int. J. Solids Struct.* **1969**, *5*, 587–605. [CrossRef]
11. Pak, R.Y.S.; Jennings, P.C. Elastodynamic response of pile under transverse excitations. *J. Eng. Mech.* **1987**, *113*, 1101–1116. [CrossRef]
12. He, R.; Pak, R.Y.S.; Wang, L.Z. Elastic lateral dynamic impedance functions for a rigid cylindrical shell type foundation. *Int. J. Numer. Anal. Met.* **2017**, *41*, 508–526. [CrossRef]
13. He, R.; Kaynia, A.M.; Zhang, J.S. A poroelastic solution for dynamics of laterally loaded offshore monopiles. *Ocean Eng.* **2019**, *179*, 337–350. [CrossRef]
14. He, R.; Kaynia, A.M.; Zhang, J.S. Influence of vertical shear stresses due to pile-soil interaction on lateral dynamic responses for offshore monopiles. *Mar. Struct.* **2019**, *64*, 341–359. [CrossRef]
15. Zdravkovic, L.; Taborda, D.M.G.; Potts, D.M.; Jardine, R.J.; Gretlund, J.S. Numerical Modelling of Large Diameter Piles under Lateral Loading for Offshore Wind Applications. In Proceedings of the International Symposium on Frontiers in Offshore Geotechnics, Oslo, Norway, 10–12 June 2015.
16. Sen, R.; Davies, T.G.; Banerjee, P.K. Dynamic analysis of piles and pile groups embedded in homogeneous soils. *Earthq. Eng. Struct. Dyn.* **1985**, *13*, 53–65. [CrossRef]
17. Latini, C.; Zania, V. Dynamic lateral response of suction caissons. *Soil Dyn. Earthq. Eng.* **2017**, *100*, 59–71. [CrossRef]

18. Tao, W.Y.; He, R.; Zheng, J.H. Analysis on horizontal-rocking vibrations of monopile supporting wind turbine. *J. Hohai Univ. Nat. Sci.* **2018**, *46*, 260–267.
19. He, R.; Ji, J.; Zhang, J.S.; Peng, W.; Sun, Z.F.; Guo, Z. Dynamic impedances of offshore rock-socketed monopiles. *J. Mar. Sci. Eng.* **2019**, *7*, 134. [CrossRef]
20. Ma, H.; Yang, J.; Chen, L. Numerical analysis of the long-term performance of offshore wind turbines supported by monopiles. *Ocean Eng.* **2017**, *136*, 94–105. [CrossRef]
21. Beuckelaers, W. Numerical Modelling of Laterally Loaded Piles for Offshore Wind Turbines. Ph.D. Thesis, University of Oxford, Oxford, UK, 2017.
22. Goit, C.S.; Saitoh, M.; Mylonakis, G.; Kawakami, H.; Oikawa, H. Model tests on horizontal pile-to-pile interaction incorporating local non-linearity and resonance effects. *Soil Dyn. Earthq. Eng.* **2013**, *48*, 175–192. [CrossRef]
23. Bhattacharya, S.; Nikitas, N.; Garnsey, J.; Alexander, N.A. Observed dynamic soil–structure interaction in scale testing of offshore wind turbine foundations. *J. Soil Dyn. Earthq. Eng.* **2013**, *54*, 47–60. [CrossRef]
24. Manna, B.; Baidya, D.K. Nonlinear dynamic response of piles under horizontal excitation. *J. Geotech. Geoenviron.* **2010**, *136*, 1600–1609. [CrossRef]
25. Elkasabgy, M.; El Naggar, M.H. Lateral vibration of helical and driven steel piles installed in clayey soil. *J. Geotech. Geoenviron.* **2018**, *144*, 6018009. [CrossRef]
26. He, R.; Zhu, T.; Ma, B.; Tao, W.Y. Dynamic Responses of Mono-piles in the Presence of Scour Holes. In Proceedings of the China-Europe Conference on Geotechnical Engineering, Vienna, Austria, 13–16 August 2018.
27. Leblanc, C.; Houlsby, G.T.; Byrne, B.W. Response of stiff piles in sand to long-term cyclic lateral loading. *Géotechnique* **2010**, *60*, 79–90. [CrossRef]
28. Shirzadeh, R.; Devriendt, C.; Bidakhvidi, M.A.; Guillaume, P. Experimental and computational damping estimation of an offshore wind turbine on a monopile foundation. *J. Wind Eng. Ind. Aerodyn.* **2013**, *120*, 96–106. [CrossRef]
29. Damgaard, M.; Ibsen, L.B.; Andersen, L.V.; Andersen, J.K.F. Cross-Wind modal properties of offshore wind turbines identified by full scale testing. *J. Wind Eng. Ind. Aerodyn.* **2013**, *116*, 94–108. [CrossRef]
30. American Petroleum Institute. *Recommended Practice for Planning, Designing and Constructing Fixed Offshore Platforms—Working Stress Design*, 21st ed.; API Recommended Practice 2A-WSD (RP2A-WSD); API: Dallas, TX, USA, 2000.
31. Burd, H.J.; Beuckelaers, W.J.A.P.; Byrne, B.W.; Gavin, K.; Houlsby, G.T.; Igoe, D.; Jardine, R.J.; Martin, C.M.; McAdam, R.A.; Muir Wood, A.; et al. New data analysis methods for instrumented medium-scale monopile field tests. *Géotechnique* **2019**, 1–28. [CrossRef]
32. McAdam, R.A.; Byrne, B.W.; Houlsby, G.T.; Beuckelaers, W.J.A.P.; Burd, H.J.; Gavin, K.; Igoe, D.; Jardine, R.J.; Martin, C.M.; Muir Wood, A.; et al. Monotonic laterally loaded pile testing in a dense marine sand at Dunkirk. *Géotechnique* **2019**, 1–34. [CrossRef]
33. Zdravković, L.; Taborda, D.M.G.; Potts, D.M.; Abadias, D.; Burd, H.J.; Byrne, B.W.; Gavin, K.; Houlsby, G.T.; Jardine, R.J.; Martin, C.M.; et al. Finite element modelling of laterally loaded piles in a stiff glacial clay till at Cowden. *Géotechnique* **2019**, 1–40. [CrossRef]
34. Taborda, D.M.G.; Zdravković, L.; Potts, D.M.; Burd, H.J.; Byrne, B.W.; Gavin, K.; Houlsby, G.T.; Jardine, R.J.; Liu, T.; Martin, C.M.; et al. Finite element modelling of laterally loaded piles in a dense marine sand at Dunkirk. *Géotechnique* **2019**, 1–47. [CrossRef]
35. Martin, C.M.; Randolph, M.F. Upper-Bound analysis of lateral pile capacity in cohesive soil. *Géotechnique* **2006**, *56*, 141–145. [CrossRef]
36. Achmus, M.; Kuo, Y.; Abdel-Rahman, K. Behavior of monopile foundations under cyclic lateral load. *Comput. Geotech.* **2009**, *36*, 725–735. [CrossRef]
37. Allotey, N.; El Naggar, M.H. A numerical study into lateral cyclic nonlinear soil-pile response. *Can. Geotech. J.* **2008**, *45*, 1268–1281. [CrossRef]
38. Gerolymos, N.; Escoffier, S.; Gazetas, G.; Garnier, J. Numerical modeling of centrifuge cyclic lateral pile load experiments. *Earthq. Eng. Eng. Vib.* **2009**, *8*, 61–76. [CrossRef]
39. Hong, Y.; He, B.; Wang, L.Z.; Wang, Z.; Ng, C.W.W.; Masin, D. Cyclic lateral response and failure mechanisms of semi-rigid pile in soft clay: Centrifuge tests and numerical modelling. *Can. Geotech. J.* **2017**, *54*, 2016–2356. [CrossRef]

40. Hardin, B.O.; Richart, F.E. Elastic wave velocities in granular soils. *J. Soil Mech. Found. Div.* **1963**, *89*, 35–65.
41. Been, K.; Jefferies, M.G. A state parameter for sands. *Géotechnique* **1985**, *35*, 99–112. [CrossRef]
42. Oda, M.; Koishikawa, I.; Higuchi, T. Experimental study of anisotropic shear strength of sand by plane strain test. *J. Jpn. Soc. Soil Mech. Found. Eng.* **1978**, *18*, 25–38. [CrossRef]
43. Hariprasad, C.; Rajashekhar, M.; Umashankar, B. Preparation of uniform sand specimens using stationary pluviation and vibratory methods. *Geotechn. Geol. Eng.* **2016**, *34*, 1909–1922. [CrossRef]
44. Cuéllar, P.; Baeßler, M.; Rücker, W. Ratcheting convective cells of sand grains around offshore piles under cyclic lateral loads. *Granul. Matter.* **2009**, *11*, 379–390. [CrossRef]
45. Ministry of Transport of the People's Republic of China. *Code for Pile Foundation in Port Engineering*; JTJ 254-1998; Ministry of Transport of the People's Republic of China: Beijing, China, 2001.
46. Hardin, B.O.; Drnevich, V.P. Shear modulus and damping in soils: Design equations and curves. *J. Soil Mech. Found. Div.* **1972**, *98*, 667–692.
47. Chopra, A.K. *Dynamics of Structures: Theory and Applications to Earthquake Engineering*; PEARSON: London, UK, 2014.
48. Seed, H.B.; Idriss, I.M. Soil moduli and damping factors for dynamic response analysis. *J. Terramech.* **1972**, *8*, 109.
49. Sørensen, S.P.H.; Brødbæk, K.T.; Møller, M.; Augustesen, A.H. *Review of Laterally Loaded Monopiles Employed as the Foundation for Offshore Wind Turbines*; Aalborg University: Aalborg, Denmark, 2012.



© 2019 by the authors. Licensee MDPI, Basel, Switzerland. This article is an open access article distributed under the terms and conditions of the Creative Commons Attribution (CC BY) license (http://creativecommons.org/licenses/by/4.0/).